ORGANOMETALLICS

Article

pubs.acs.org/Organometallics

A Neutrally Charged Trimethylmanganese(III) Complex: Synthesis, Characterization, and Disproportionation Chemistry

Madelyn M. Stalzer,[†] Joshua Telser,[‡] Jurek Krzystek,[§] Alessandro Motta,[∥] Massimiliano Delferro,*[,⊥] and Tobin J. Marks*[,†]

[†]Department of Chemistry, Northwestern University, Evanston, Illinois 60208, United States

[‡]Department of Biological, Chemical, and Physical Sciences, Roosevelt University, Chicago, Illinois 60605, United States

[§]National High Magnetic Field Laboratory, Florida State University, Tallahassee, Florida 32310, United States

[∥]Dipartimento di Chimica and INSTM UdR Roma, Università degli Studi di Roma "La Sapienza" P.le A. Moro 5, Roma, I-00185, Italy

[⊥]Chemical Sciences & Engineering Division, Argonne National Laboratory, Argonne, Illinois 60439, United States

Supporting Information

ABSTRACT: The synthesis and properties of an unusual, neutrally charged and volatile *N*,*N*,*N*′,*N*′-tetramethylethylenediamine trimethyl manganese(III) complex, (TMEDA)$MnMe_3$, are described, along with its facile disproportionation to the corresponding Mn(II) and Mn(IV) complexes. Characterization by single-crystal XRD, UV−vis spectroscopy, high-frequency and -field EPR (HFEPR), magnetic susceptibility, and density functional theory (DFT) computations indicate that the (TMEDA)$MnMe_3$ electronic structure can be described as largely square pyramidal Mn(III) centered. The paucity of manganese(III) polyalkyls and the simplicity and reactivity of this compound implicate it as a potentially useful synthetic building block.

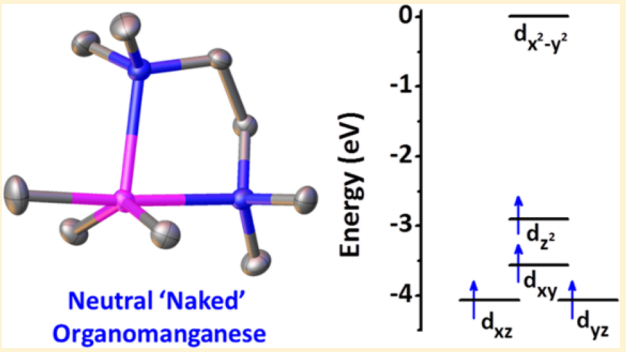

INTRODUCTION

The capacity of manganese to exhibit a wide range of formal oxidation states (−I to +VII), along with its ability in oscillating among them, makes Mn ubiquitous as a potent catalyst in both biology and chemistry.[1] This is demonstrated by its role in the O_2-evolving complex of photosystem II[2] and utility in many chemical transformations, including C−H bond oxidation,[3] alkene epoxidation,[4] and electrochemical CO_2 reduction.[5] Many of these active manganese centers are coordinated by bulky Lewis base,[6] porphyrin,[3a,7] or salen[4] type ligands that act to stabilize the oscillating formal Mn oxidation state. The synthesis of discrete, mononuclear manganese polyalkyls has, however, proven challenging due to the inability of carbon-based σ-donor ligands to electronically stabilize the redox-labile metal centers, leading to extreme O_2, water, and temperature sensitivity, with only a handful of manganese alkyls being reported.[8] Specifically, for high-valent Mn(III) and Mn(IV), for which the binary metal halides are thermally unstable,[9] the lack of traditional precursors amplifies the synthetic challenge. Note that many of the manganese hydrocarbyls known in these high oxidation states bear a net formal negative charge at the metal center and require charge-balancing counterions (see Table 1 for selected examples of Mn(III)).

With the goal of discovering novel manganese hydrocarbyl structures and characterizing their chemical and physical properties, our laboratory was enticed by the challenge of stabilizing neutrally charged Mn(III) polyalkyls with simple organic ancillary ligands. The synthesis of a manganese(III) polyalkyl was first achieved by reacting manganese(III) acetylacetonate with methyllithium in the presence of the stabilizing bidentate amine *N*,*N*,*N*′,*N*′-tetramethylethylenediamine (TMEDA) to form $\{[Li(TMEDA)]_2\}^{2+}[MnMe_5]^{2-}$.[10] It was also demonstrated that the comproportionation of the corresponding Mn(II) and Mn(IV) complexes is a viable

Table 1. Selected Mn(III) Polyhydrocarbyls from the Literature

compound	ref
$\{[Li(TMEDA)]_2\}^{2+}[MnMe_5]^{2-}$	10
$[Li(TMEDA)_2]^+[MnMe_4]^-$	10
$MnBr_2(2,4,6\text{-}C_6H_2Me_3)(PMe_3)_2$	11
$[K(py)_2]^+[Mn(C_4H_8)_2py]^-$ [a]	12
$[MnMe_2(dmpe)_2]^+[AlMe_4]^-$ [b]	13
$[Mg(THF)_6]^{2+}\{[Mn(C_6F_5)_4]_2\}^{2-}$ [c]	14

[a]py = pyridine. [b]dmpe = 1,2-bis(dimethylphosphine)ethane. [c]THF = tetrahydrofuran.

Received: May 25, 2016

DOI: 10.1021/acs.organomet.6b00422
Organometallics XXXX, XXX, XXX−XXX

synthetic route to the same product.[10] Here, modification of the former route enables the synthesis of the first neutrally charged, volatile trimethylmanganese(III) complex, the molecular and electronic structures of which are elucidated here via diffraction, spectroscopic, and computational analyses.

RESULTS AND DISCUSSION

The title compound, (*N*,*N*,*N*′,*N*′-tetramethylethylenediamine)-trimethylmanganese(III) ((TMEDA)$MnMe_3$, **1**), was synthesized by the reaction of $Mn(acetylacetonate)_3$ (1.0 g, 2.84 mmol) with methyllithium (5.75 mL, 1.6 M in diethyl ether, 9.20 mol) in the presence of TMEDA (0.45 mL, 3.00 mmol) at −78 °C in diethyl ether. After the reaction mixture was warmed to 25 °C, colorless Li(acac) was removed by cannula filtration, and the deep red filtrate was dried in vacuo. Addition of pentane and subsequent filtration followed by concentration and storage at −40 °C afforded X-ray-quality deep red needle-like crystals. Although combustion analysis proved difficult due to the extreme sensitivity of **1** (vide infra), powder X-ray diffraction experiments agree very well with the pattern predicted from the single-crystal data, supporting the purity of the bulk material. Compound **1** is volatile and readily sublimes at 40 °C/100 mTorr, suggesting potential application in vapor deposition film growth processes.[15] It is interesting to note that this synthesis differs only slightly from that of $\{[Li(TMEDA)]_2\}^{2+}[MnMe_5]^{2-}$ by Morris and Girolami,[10] where excess methyllithium (10 equiv) was added to a suspension of $Mn(acac)_3$ followed by washing with pentane and subsequent reaction with TMEDA in ether. The presence of TMEDA during methyllithium addition in the present synthesis likely stabilizes manganese(III) intermediates and prevents addition of more than three alkyl nucleophiles to the metal center.

Single-crystal X-ray diffraction analysis of **1** reveals a highly distorted five-coordinate structure (Figure 1a). According to a

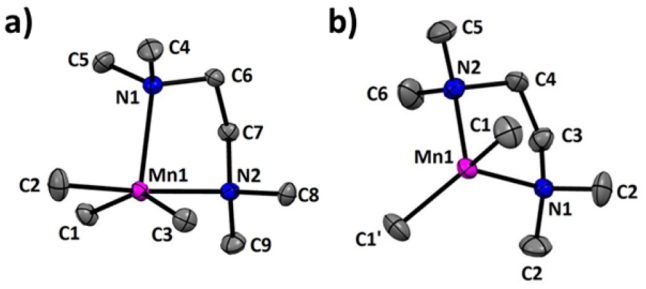

Figure 1. ORTEP plots (50% thermal ellipsoids) of the X-ray crystal structures of complexes (a) **1** and (b) **2** (H atoms deleted for clarity). Selected bond distances (Å) and angles (deg) for **1**: Mn1−N1 = 2.3280(8), Mn1−N2 = 2.2449(9), Mn1−C1 = 2.1016(10), Mn1−C2 = 2.0580(13), Mn1−C3 = 2.1183(12); N1−Mn1−N2 = 79.88(3), C1−Mn−C3 = 148.53(5), N1−Mn1−C2 = 176.27(5). Selected bond distances (Å) and angles (deg) for **2**: Mn1−N1 = 2.4537(17), Mn1−N2 = 2.3760(17), Mn1−C1 = 2.0332(16); N1−Mn1−N2 = 75.25(5), C1−Mn−C1′ = 132.57(12).

Reedijk analysis,[16] $\tau = 0.46$ ($\tau = 0$ for a perfect square pyramid and $\tau = 1$ for a perfect trigonal bipyramid), indicative of severe distortion from either trigonal-bipyramidal or square-pyramidal geometries. Both are common geometries for known Mn(III) complexes, and hybrid geometries are common for compounds where ligands present steric restrictions.[17] For **1**, the small TMEDA ligand bite angle, combined with the steric repulsion of the three methyl groups, likely causes this geometric distortion. Furthermore, the two trans methyl groups exhibit significant distortion from ideal planar (180°) or trigonal (120°) coordination, having a C1−Mn−C3 angle of 148.53(5)°. An elongation of the apical Mn1−N1 bond (2.3280(8) Å) is also observed versus the basal Mn−N2 bond (2.2449(9) Å), likely due to pseudo-Jahn−Teller distortion, in good agreement with DFT modeling (vide infra). The Mn−C distances of 2.08−2.13 Å are unremarkable in comparison to those of related methylmanganese(IV) and alkylmanganese(III) complexes (Table 1).

Concerning reactivity and stability, complex **1** reacts pyrophorically with air and water. Additionally, slow decomposition is observed at 25 °C in the solid state under an inert atmosphere over the course of 1 week. In solution, decomposition occurs more readily (1−2 days). Bimolecular disproportionation is the proposed pathway of the decomposition process,[10] producing (TMEDA)$MnMe_2$ (**2**) and (TMEDA)$MnMe_4$ (**3**) (eq 1). Orange X-ray-quality crystals of **2** are obtained by recovering the filtrate from the synthesis of **1** and storing it at −40 °C for an additional week. Single-crystal X-ray analysis of **2** reveals a distorted-tetragonal coordination geometry, typical of four-coordinate Mn(II) complexes (Figure 1b). The TMEDA bite angle again manifests itself in the small N1−Mn−N2 angle of 75.25(5)°, while the two alkyl groups subtend a large C1−Mn−C1′ angle of 132.5(1)°. Similar patterns are observed in $[Mn(CH_2SiMe_3)_2(dmpe)]$[18] and $[Mn(CH_2CMe_2Ph)_2(bipy)]$,[19] which likewise reflect the steric constraints of the bidentate ligands. The Mn−C bond distances in **2** are symmetry-equivalent and have a value of 2.0032(16) Å, which, to our knowledge, is the shortest Mn^{II}−C bond distance reported to date. An Evans method analysis[20] reveals $\mu_{eff} = 5.52$ μ_B, in good agreement with the theoretical value of $\mu_{eff} = 5.92$ μ_B for high-spin ($S = 5/2$) Mn(II). In a frozen toluene solution, **2** gives an X-band EPR signal with $D \gtrsim 0.1$ cm^{-1}, also consistent with high-spin Mn(II) (see Figure S4 in the Supporting Information).

$$\underset{\mathbf{1}}{2(\text{TMEDA})MnMe_3} \rightarrow \underset{\mathbf{2}}{(\text{TMEDA})MnMe_2} + \underset{\mathbf{3}}{(\text{TMEDA})MnMe_4} \quad (1)$$

Attempts to isolate and characterize compound **3** were unsuccessful.[21] It is likely that **3** exists as a transient species that undergoes further rapid decomposition to **2**, similar to other proposed Mn(IV) intermediates.[22]

Investigation of the electronic structure of **1** was next pursued to elucidate what, if any, affect the σ-donating methyl ligands have on the metal ion. An Evans method analysis of **1** yields $\mu_{eff} = 4.86$ μ_B, corresponding to the spin-only value for $S = 2$ with $g = 1.984$, a reasonable value for Mn(III), with a less than half-filled shell. The UV−visible absorption spectrum for **1** (0.15 mM in pentane) is shown in Figure 2a. Two peaks and a shoulder are observed at 305, 348, and 428 nm, with $\varepsilon = 8500$, 7900, and 1400 L/(mol cm), respectively. All three bands are assigned to d−d transitions since ligand−metal charge transfer is unlikely in this energy range for the σ-bonding methyl ligands or the datively coordinated diamine. Additionally, UV/visible/near-IR spectroscopic analysis reveals no additional features in the 200−3500 nm range. Assignment of the d−d transitions (Figure 2b) then provides a picture of the d orbital splitting, which correlates well with the distorted structure as a

DOI: 10.1021/acs.organomet.6b00422
Organometallics XXXX, XXX, XXX−XXX

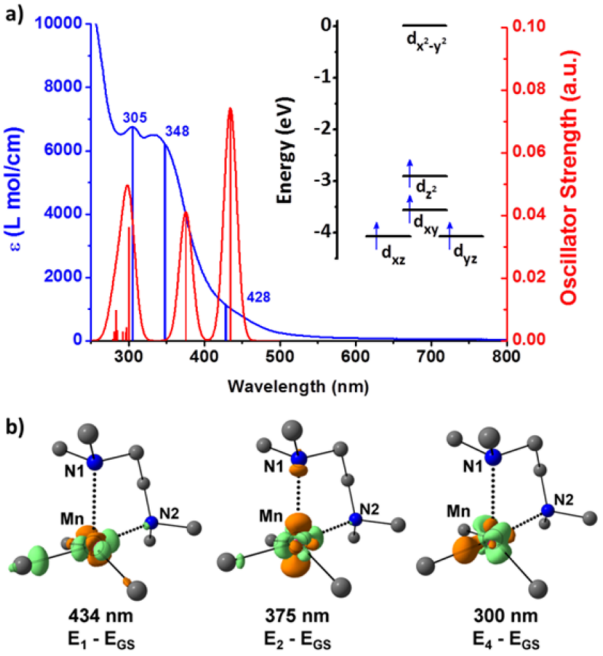

Figure 2. (a) Experimental and DFT computed UV−visible spectra of **1** as a 0.15 mM pentane solution, with the inset showing calculated frontier orbital splittings for d^4 Mn(III) in a distorted-square-pyramidal geometry. (b) Calculated isosurfaces of the electron density difference between the ground (orange) and excited (green) states of the DFT computed UV−vis transitions for **1**. Hydrogen atoms are omitted for clarity.

combination of classical crystal field square-pyramidal and trigonal-bipyramidal splittings. Furthermore, DFT calculations on the excited states of **1** agree with the observed electronic transitions, predicting three bands at 299, 374, and 434 nm. The differences in electron density of the excited and ground states (Figure 2b) indicate that the transitions are all associated with d−d charge transfer processes, and a natural transition orbital (NTO) analysis reveals that the band at 434 nm mainly involves HOMO transfer to the LUMO, while the other two transitions arise due to transfer from orbitals just below the HOMO to the LUMO.

To further interrogate the electronic structure of complex **1**, electron paramagnetic resonance (EPR) experiments were carried out. Due to the integer spin leading to a non-Kramers ion, high-frequency and high-field EPR (HFEPR) was applied, and **1** gives strong responses in the frequency range 50−400 GHz and the temperature range 10−284 K. Figure 3 shows the low-temperature (10 K) spectrum at 216 GHz (for additional frequencies, see Figures S5−S7 in the Supporting Information). The spectra reveal narrow resonances spread over the entire field range, attributable to Mn(III), and a broader single line centered on $g \approx 2$, attributed to small amounts of the Mn(II) disproportionation products (vide infra).[23,24] The Mn(III) spectra aided by simulations show that they are nearly perfect powder patterns of the quintet ($S = 2$) state characterized by an axial zero-field splitting tensor (D) of ~ -2.19 cm^{-1}. Accurate values of the zero-field splitting (zfs) parameters were obtained via the tunable-frequency EPR procedure.[25] In brief, this procedure involves plotting the resonant magnetic fields of spectral features (turning points) observed in the EPR powder pattern versus the frequency employed. The simultaneous best fit to all of these resonances is then performed, with these

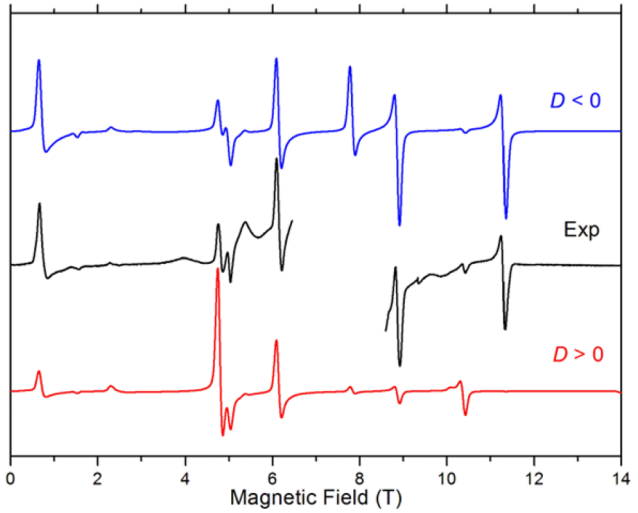

Figure 3. Powder EPR spectra of complex **1** at 10 K and 216 GHz (black trace) accompanied by simulations (colored traces) using an $S = 2$ spin Hamiltonian with $|D| = 2.195$ cm^{-1}, $E = 0$, and $g = 2.00$: (blue trace) $D < 0$; (red trace) $D > 0$. The broad and unresolved resonance due to traces of the Kramers species (Mn(II) and Mn(IV)) at $g \approx 2.00$ (~7.7 T) is omitted from the experimental spectrum for clarity.[23]

calculated transitions shown on the plot as continuous lines. The resulting such 2D field vs frequency (or energy) map of turning points seen for **1** at 10 K is shown in Figure 4 together

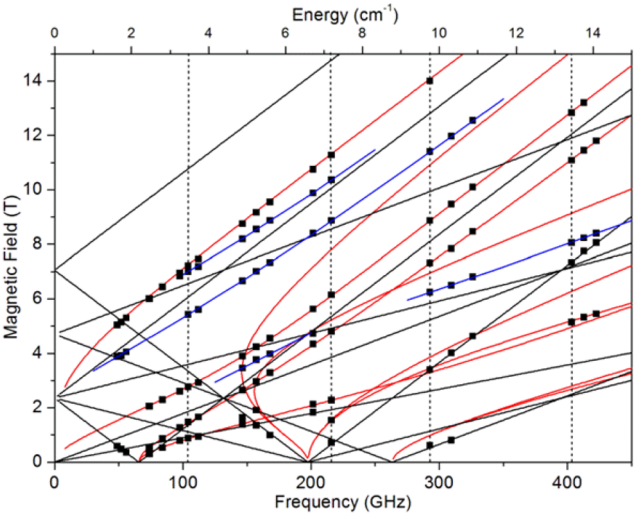

Figure 4. 2D map of turning points in the HFEPR spectra of **1** at 10 K (black squares) together with simulations using the spin Hamiltonian parameters in Table 2 (lines): (black lines) turning points with magnetic field B_0 parallel to the z axis of the zfs tensor; (red lines) B_0 perpendicular to z; (blue lines) off-axis turning points. The dashed vertical lines correspond to the frequencies at which spectra shown in Figures S5, S6, and S7 in the Supporting Information and Figure 3 above, in increasing frequency order, are shown.

with simulations using best-fit spin Hamiltonian parameters that are given in Table 2. Addition of the fourth-rank zfs parameters only slightly improves the fit,[26] yielding a B^4_4 value barely twice the statistical error: $-[10(5)] \times 10^{-4}$ cm^{-1}. The zfs parameter D decreases in magnitude to -2.08 cm^{-1} while E remains strictly 0 at 284 K (Figure S8 and S9 in the Supporting Information). Concerning the value of D, a number of Mn(III) coordination complexes have been studied by HFEPR and their

DOI: 10.1021/acs.organomet.6b00422
Organometallics XXXX, XXX, XXX−XXX

Table 2. Spin Hamiltonian Parameters of the $S = 2$ Mn(III) in Complex 1

T (K)	D (cm^{-1})	E (cm^{-1})	$g_\perp$	$g_\parallel$	B^4_4 (10^{-4} cm^{-1})
10	−2.178(4)	0.002(2)	2.004(2)	2.014(4)	−10(5)
100	−2.17	0	2.00	2.00	
284	−2.08	0	2.00	2.00	

zfs parameters have been accurately determined; they are given in Table S7 in the Supporting Information. These complexes are almost exclusively five- and six-coordinate with N, O, or halide ligands. Note that complex **1** represents a heretofore unexamined inner coordination sphere in terms of having three alkyl C donors. Nevertheless, the magnitude of D and its negative sign are quite similar to those reported for square-planar/-pyramidal Mn(III) tetrapyrrole (porphyrin or corrole) systems, which also exhibit essentially axial symmetry with D in the range −2.3 to −2.7 cm^{-1} (Table S7).[23,27] In the case of **1**, the key molecular structure feature that determines the electronic structure is the elongation of the axial Mn−N1 bond that distinguishes the x and y axes from the z axis (Mn−N1), leading to $D < 0$ and corresponding to a $d_{x^2-y^2}$ ground state (see Figure 2a, inset). Positive D values, in contrast, are attributable to a d_{z^2} ground state, as seen in a Mn(III)-doped oxide material.[28] Ab initio calculations[29] provide a D value of −2.19 cm^{-1}, in excellent agreement with experiment (−2.178(4) cm^{-1}). Additionally, a ligand-field theory calculation using the full d^4 basis set, analogous to complete active space self consistent field method based on 4 electrons and 5 orbitals (CASSF(4,5)), with the single-electron d orbital energies as given in the MO scheme in Figure 2a and with spin−orbit coupling and interelectronic repulsion parameters at 70% of their free ion values, yields $D = -2.30$ cm^{-1} with no E and a very small fourth-order zfs (see the Supporting Information). Furthermore, the g values from ab initio calculations agree with experiment in terms of being roughly axial ($g_x \approx g_y = g_\perp$) and with $g_\parallel$ (g_z) > $g_\perp$ > g_e. Thus, it can be concluded that, despite the distorted geometry of **1**, the experimentally and theoretically obtained D values indicate a square-pyramidal behavior, analogous to Mn(porphyrin/corrole)X (X = halide, alkoxide, phosphine oxide) species.[27b−d,30]

CONCLUSIONS

These results reveal how slight modifications to known synthetic procedures (e.g., order of reagent addition) can result in interesting new compounds such as the neutrally charged volatile trimethylmanganese(III) compound described here. The spectroscopic signatures seen in the UV−vis and EPR spectra of **1** confirm the presence of a d^4 Mn(III) species and indicate the metal-centered nature of the unpaired electrons, while also providing one of the first benchmark values for the zfs parameters of organomanganese(III). The ease of synthesis of **1** lends itself well to further derivatization, with potential application as a synthon for organomanganese compounds with more complex ligand systems to serve as catalysts for organic substrate functionalization. Additionally, the volatility and high reactivity of **1** present opportunities for application as a precursor for film growth processes. These possibilities are currently under investigation.

EXPERIMENTAL SECTION

General Considerations. All procedures for air- and moisture-sensitive compounds were carried out with rigorous exclusion of O_2 and moisture in flame- or oven-dried Schlenk-type glassware interfaced to a dual-manifold Schlenk line or a high-vacuum (10^{-5}−10^{-6} Torr) line or in an Ar-filled MBraun glovebox with a high-capacity recirculator (<1 ppm of O_2). Argon (Airgas, prepurified) was purified by passage through MnO/vermiculite and Davison 4 Å molecular sieve columns. All hydrocarbon solvents were distilled from Na/K alloy and stored in resealable flasks. Diethyl ether was dried over sodium, using benzophenone indicator, and freshly distilled before use. All other starting materials were purchased from Sigma-Aldrich Chemical Co. and used as received.

Physical and Analytical Measurements. UV/visible/near-IR measurements were acquired on a PerkinElmer LAMBDA 1050 double-beam spectrophotometer, using a quartz cuvette equipped with a Teflon seal-lined screw top. FTIR spectra were collected on ground samples in Nujol mulls using a Bruker Tensor 37 FTIR instrument with ATR attachment. Elemental analyses were performed by Midwest Microlab, Indianapolis, IN, for % C, N, H.

X-ray Data Collection, Structure Solution, and Refinement. Single crystals of **1** and were crystallized from pentane at −40 °C, mounted in inert oil, and transferred to a cold nitrogen gas stream of a Bruker Kappa APEX CCD area detector equipped with a Mo Kα microsource. The crystal was maintained at 100.0 K during data collection. Powder X-ray diffraction patterns were collected on the same instrument, using ψ scans of 180°. The powder X-ray diffraction sample was prepared by finely grinding **1** and mounting it on a loop in inert oil. Predicted PXRD patterns were calculated on the basis of the single-crystal data using Mercury 3.5 software.

HFEPR Instrumentation and Analysis. HFEPR spectra were recorded at the Electron Magnetic Resonance (EMR) Facility, National High Magnetic Field Laboratory (NHMFL, Tallahassee, FL, USA), using a spectrometer that is identical with that described previously[31] except for the source, which is currently a solid-state device (Virginia Diodes, Charlottesville, VA, USA) operating at a base frequency of 12−14 GHz with a cascade of frequency multipliers. Phase-sensitive detection was used, with the magnetic field modulated at 50 kHz. The ac response was fed into a Stanford SR830 lock-in amplifier to obtain a dc signal. Low-temperature control was provided by a continuous flow cryostat (Oxford Instruments, Oxford, U.K.). HFEPR spectra were simulated using a locally written program, SPIN, available from A. Ozarowski, using a standard spin Hamiltonian:[26]

$$\mathcal{H} = \beta_e B \cdot g \cdot \hat{S} + D\left(\hat{S}_z^{\,2} - \frac{1}{3}S(S+1)\right) + E(\hat{S}_x^{\,2} - \hat{S}_y^{\,2})$$

All samples were run as either finely crushed powders or compressed Nujol mulls in polyethylene sample tubes. Both preparations yielded identical results.

Synthetic Details. *Trimethyl(N,N,N′,N′-tetramethylethylenediamine)manganese(III) (1).* In a 50 mL Schlenk-type flask was placed manganese acetylacetonate (1.00 g, 2.84 mmol). The black solid was suspended in 40 mL of diethyl ether, and then *N*,*N*,*N*′,*N*′-tetramethylethylenediamine (0.45 mL, 3.0 mmol) was added. At −78 °C, a solution of 1.6 M methyllithium in diethyl ether (5.75 mL, 9.20 mmol) was added slowly via syringe. The solution was then stirred for 30 min, warmed to room temperature, and stirred for an additional 1 h. The deep red solution was then filtered, the solvent was replaced with pentane, and this mixture was filtered again. The pentane solution was then concentrated and stored at −40 °C overnight to give 0.184 g (30% yield) of deep red needlelike crystals. A satisfactory elemental analysis for **1** was not obtained due to decomposition during shipping and/or sample preparation. IR (cm^{-1}, Nujol mull): 2794 m, 1407 vw, 1354 w, 1286 s, 1248 w, 1183 m, 1160

DOI: 10.1021/acs.organomet.6b00422
Organometallics XXXX, XXX, XXX−XXX

s, 1122 s, 1108 vs, 1096 w, 1077 m, 1063 m, 1042 w, 1023 m, 1013 vs, 1003 m, 951 vs, 930 m, 793 vs, 768 s.

Dimethyl(N,N,N′,N′-tetramethylethylenediamine)manganese(II) (2). A solution of **1** in pentane was stored at −0 °C for 5 days until orange X-ray-quality crystals formed. Crystals were isolated by filtration (36% yield). Anal. Calcd: C, 47.8; H, 11.0; N, 13.9. Found: C, 47.56; H, 11.05; N, 13.79. IR (cm^{-1}, Nujol mull): 2801 m, 2779 m, 1410 vw, 1355 w, 1288 s, 1248 m, 1185 m, 1162 s, 1128 s, 1109 s, 1064 m, 1046 w, 1031 m, 1014 m, 948 vs, 932 vw, 790 vs, 768 m. UV−vis (pentane): λ_{max} 361 nm (ε = 210).

Computational Details. Geometry optimizations of the Mn(III) and Mn(II) complexes were carried out starting from XRD parameters. Calculations were performed by adopting the B3LYP hybrid functional.[32] The standard all-electron 6-311+G** basis[33] was used for all atoms. Molecular geometry optimization of stationary points was carried out without symmetry constraints and used analytical gradient techniques. Frequency analysis was performed to verify the geometric stability. Solvent effects were modeled using the polarized continuum (overlapping spheres) formalism (PCM) of Tomasi and co-workers.[34] Excited-state calculations were performed on the optimized geometry using the time-dependent DFT (TD-DFT) method and adopting the long-range corrected version of the B3LYP functional to better take into account eventual charge transfer processes between the metal center and ligands.[35] The *g* values were evaluated by taking into account the anisotropic hyperfine coupling constants.[36] All of these calculations were performed using the G09 code.[37] Theoretical evaluation of the zero field splitting parameters required a more sophisticated multireference ab initio approach. In this case the complete active space self consistent field (CASSCF) method based on 4 electrons and 5 orbitals, CAS(4,5), reference was considered and the interactions of 5 quintet and 35 triplet states were included in the state averaged CASSCF framework.[38] Equal weights for all excited states were considered. The spin−orbit coupling was evaluated with the effective Hamiltonian theory approach. The wave function was evaluated using the DFT optimized geometry and employed the def2-sv(p) basis set.[39] This calculation was carried out using the ORCA code.[29b]

Ligand-Field Theory Analysis. Calculations using the entire d^4 basis set were performed using the locally written program DDN. Free ion values for the spin−orbit coupling (SOC) parameter, ζ, and Racah interelectronic repulsion parameters, *B* and *C*, were taken from those reported by Brorson, Bendix, and co-workers.[40] These were scaled down to 70% to reflect the metal−ligand covalency of compound **1**. The single-electron d orbital energy levels given in the MO scheme of Figure 2a were used for the bonding aspects of the calculation (see the Supporting Information for input parameters and results for the ground-state spin quintet).

■ ASSOCIATED CONTENT

Supporting Information

The Supporting Information is available free of charge on the ACS Publications website at DOI: 10.1021/acs.organomet.6b00422.

Details of crystallographic data, PXRD, EPR spectra, and computational methods (PDF)

Crystallographic data (CIF)

Crystallographic data (CIF)

■ AUTHOR INFORMATION

Corresponding Authors

*E-mail for M.D.: delferro@anl.gov.

*E-mail for T.J.M.: t-marks@northwestern.edu.

Notes

The authors declare no competing financial interest.

■ ACKNOWLEDGMENTS

This work was supported as part of the Center for Electrochemical Energy Science, an Energy Frontier Research Center funded by the U.S. Department of Energy, Office of Science, Basic Energy Sciences under award number DE-AC02−06CH11. HFEPR studies were supported by the NHMFL, which is funded by the NSF through a Cooperative Agreement DMR 1157490, the State of Florida, and the U.S. Department of Energy. Computational resources supporting this work were provided by the Northwestern University Quest High Performance Computing cluster (M.D.) and CINECA award N. HP10CRFT69 2016 under the ISCRA initiative (A.M.). Dr. A. Ozarowski is acknowledged for his EPR simulation and fitting program SPIN.

■ REFERENCES

(1) (a) Wikaira, J.; Gorun, S. M. In *Bioinorganic Catalysis*, 2nd ed.; Reedijk, J., Bouwman, E., Eds.; CRC Press: New York, NY, USA, 1999. (b) Khusnutdinov, R.; Bayguzina, A.; Dzhemilev, U. *Russ. J. Org. Chem.* **2012**, *48*, 309−348. (c) Manrique, E.; Poater, A.; Fontrodona, X.; Sola, M.; Rodriguez, M.; Romero, I. *J. Chem. Soc., Dalton Trans.* **2015**, *44*, 17529−17543. (d) Daneshmand, P.; Schaper, F. *J. Chem. Soc., Dalton Trans.* **2015**, *44*, 20449−20458.

(2) Yano, J.; Yachandra, V. *Chem. Rev.* **2014**, *114*, 4175−4205.

(3) (a) Paradine, S. M.; Griffin, J. R.; Zhao, J.; Petronico, A. L.; Miller, S. M.; Christina White, M. *Nat. Chem.* **2015**, *7*, 987−994. (b) Shul'pin, G. B. *J. Chem. Soc., Dalton Trans.* **2013**, *42*, 12794−12818.

(4) McGarrigle, E. M.; Gilheany, D. G. *Chem. Rev.* **2005**, *105*, 1563−1602.

(5) (a) Bourrez, M.; Molton, F.; Chardon-Noblat, S.; Deronzier, A. *Angew. Chem.* **2011**, *123*, 10077−10080. (b) Sampson, M. D.; Kubiak, C. P. *J. Am. Chem. Soc.* **2016**, *138*, 1386−1393. (c) Walsh, J. J.; Neri, G.; Smith, C. L.; Cowan, A. J. *Chem. Commun.* **2014**, *50*, 12698−12701.

(6) (a) Lewis, R. A.; Wu, G.; Hayton, T. W. *Inorg. Chem.* **2011**, *50*, 4660−4668. (b) Lewis, R. A.; Morochnik, S.; Chapovetsky, A.; Wu, G.; Hayton, T. W. *Angew. Chem.* **2012**, *124*, 12944−12947.

(7) (a) Weiss, R.; Bulach, V.; Gold, A.; Terner, J.; Trautwein, A. X. *JBIC, J. Biol. Inorg. Chem.* **2001**, *6*, 831−845. (b) Liu, W.; Groves, J. T. *Acc. Chem. Res.* **2015**, *48*, 1727−1735.

(8) (a) Bower, B. K.; Tennent, H. G. *J. Am. Chem. Soc.* **1972**, *94*, 2512−2514. (b) Girolami, G. S.; Morris, R. H. In *Comprehensive Organometallic Chemistry II*; Abel, E. W., Stone, F. G. A., Wilkinson, G., Eds.; Elsevier Science: Oxford, U.K., 1995; Vol. *6*, pp 127−150.

(9) (a) Funk, H.; Kreis, H. *Z. Anorg. Allg. Chem.* **1967**, *349*, 45−49. (b) Fisher, W. W. *J. Chem. Soc., Trans.* **1878**, *33*, 409−415.

(10) Morris, R. J.; Girolami, G. S. *Organometallics* **1991**, *10*, 792−799.

(11) Morris, R. J.; Girolami, G. S. *Organometallics* **1991**, *10*, 799−804.

(12) Jonas, K.; Burkart, G.; Häselhoff, C.; Betz, P.; Krüger, C. *Angew. Chem., Int. Ed. Engl.* **1990**, *29*, 322−323.

(13) Komiya, S.; Kimura, T.; Kaneda, M. *Organometallics* **1991**, *10*, 1311−1316.

(14) Forniés, J.; Martín, A.; Martín, L. F.; Menjón, B.; Zhen, H.; Bell, A.; Rhodes, L. F. *Organometallics* **2005**, *24*, 3266−3271.

(15) (a) Koponen, S. E.; Gordon, P. G.; Barry, S. T. *Polyhedron* **2016**, *108*, 59. (b) Wang, X.; Yushin, G. *Energy Environ. Sci.* **2015**, *8*, 1889−1904.

(16) Addison, A. W.; Rao, T. N.; Reedijk, J.; van Rijn, J.; Verschoor, G. C. *J. Chem. Soc., Dalton Trans.* **1984**, 1349−1356.

(17) Latten, J. L.; Dickson, R. S.; Deacon, G. B.; West, B. O.; Tiekink, E. R. T. *J. Organomet. Chem.* **1992**, *435*, 101−108.

(18) Andersen, R. A.; Berg, D. J.; Fernholt, L.; Faegri, K.; Green, J. C.; Haaland, A.; Lappert, M. F.; Leung, W.-P.; Rypdal, K. *Acta Chem. Scand.* **1988**, *42a*, 554−562.

DOI: 10.1021/acs.organomet.6b00422
Organometallics XXXX, XXX, XXX−XXX

(19) Cámpora, J.; Palma, P.; Pérez, C. M.; Rodríguez-Delgado, A.; Álvarez, E.; Gutiérrez-Puebla, E. *Organometallics* **2010**, *29*, 2960−2970.
(20) Shoemaker, D. P.; Garland, C. W.; Nibler, J. W. *Experiments in Physical Chemistry*, 5th ed.; McGraw-Hill: New York, 1989.
(21) An Evans method analysis of a deep red oil remaining after isolation of **2** at −40 °C gave μ_{eff} = 3.7 μ_B, which agrees with μ_{eff} = 3.87 μ_B expected for S = 3/2 d^3 Mn(IV); however, further characterization was fruitless.
(22) (a) Cahiez, G.; Bernard, D.; Normant, J. F. *J. Organomet. Chem.* **1976**, *113*, 99−106. (b) Cahiez, G.; Moyeux, A.; Buendia, J.; Duplais, C. *J. Am. Chem. Soc.* **2007**, *129*, 13788−13789.
(23) Krzystek, J.; Ozarowski, A.; Telser, J. *Coord. Chem. Rev.* **2006**, *250*, 2308−2324.
(24) Decomposition upon shipping to the National High Magnetic Field Laboratory in Tallahassee, FL, even under refrigeration, was found to be unavoidable.
(25) Krzystek, J.; Zvyagin, S. A.; Ozarowski, A.; Trofimenko, S.; Telser, J. *J. Magn. Reson.* **2006**, *178*, 174−183.
(26) Abragam, A.; Bleaney, B. *Electron Paramagnetic Resonance of Transition Ions (Oxford Classic Texts in the Physical Sciences)*; Oxford University Press: Oxford, U.K., 2012. The fourth order term is

$$B_4^4\hat{O}_4^4 = \frac{1}{2}(\hat{S}_+^4 + \hat{S}_-^4)$$

For clarity, this term is not included in eq 1.
(27) (a) Pascual-Álvarez, A.; Vallejo, J.; Pardo, E.; Julve, M.; Lloret, F.; Krzystek, J.; Armentano, D.; Wernsdorfer, W.; Cano, J. *Chem. - Eur. J.* **2015**, *21*, 17299−17307. (b) Kennedy, B. J.; Murray, K. S. *Inorg. Chem.* **1985**, *24*, 1557−1560. (c) Krzystek, J.; Telser, J.; Pardi, L. A.; Goldberg, D. P.; Hoffman, B. M.; Brunel, L.-C. *Inorg. Chem.* **1999**, *38*, 6121−6129. (d) Krzystek, J.; Telser, J.; Hoffman, B. M.; Brunel, L.-C.; Licoccia, S. *J. Am. Chem. Soc.* **2001**, *123*, 7890−7897.
(28) Krzystek, J.; Telser, J.; Li, J.; Subramanian, M. A. *Inorg. Chem.* **2015**, *54*, 9040−9045.
(29) (a) Deng, Y.-F.; Han, T.; Wang, Z.; Ouyang, Z.; Yin, B.; Zheng, Z.; Krzystek, J.; Zheng, Y.-Z. *Chem. Commun.* **2015**, *51*, 17688−17691. (b) Neese, F. *WIREs Comput. Mol. Sci.* **2012**, *2*, 73−78. (c) Atanasov, M.; Ganyushin, D.; Pantazis, D. A.; Sivalingam, K.; Neese, F. *Inorg. Chem.* **2011**, *50*, 7460−7477.
(30) Bendix, J.; Gray, H. B.; Golubkov, G.; Gross, Z. *Chem. Commun.* **2000**, 1957−1958.
(31) Hassan, A. K.; Pardi, L. A.; Krzystek, J.; Sienkiewicz, A.; Goy, P.; Rohrer, M.; Brunel, L. C. *J. Magn. Reson.* **2000**, *142*, 300−312.
(32) Becke, A. D. *J. Chem. Phys.* **1993**, *98*, 5648−5652.
(33) (a) Krishnan, R.; Binkley, J. S.; Seeger, R.; Pople, J. A. *J. Chem. Phys.* **1980**, *72*, 650−654. (b) Hay, P. J. *J. Chem. Phys.* **1977**, *66*, 4377−4384.
(34) Tomasi, J.; Mennucci, B.; Cammi, R. *Chem. Rev.* **2005**, *105*, 2999−3094.
(35) Yanai, T.; Tew, D. P.; Handy, N. C. *Chem. Phys. Lett.* **2004**, *393*, 51−57.
(36) Rega, N.; Cossi, M.; Barone, V. *J. Chem. Phys.* **1996**, *105*, 11060−11067.
(37) Frisch, M. J., et al. *Gaussian 09, Revision E*; Gaussian, Inc., Wallingford, CT, 2009.
(38) Neese, F. *J. Am. Chem. Soc.* **2006**, *128*, 10213−10222.
(39) Weigend, F.; Ahlrichs, R. *Phys. Chem. Chem. Phys.* **2005**, *7*, 3297−3305.
(40) (a) Brorson, M.; Schaeffer, C. E. *Inorg. Chem.* **1988**, *27*, 2522−2530. (b) Bendix, J.; Brorson, M.; Schaffer, C. E. *Inorg. Chem.* **1993**, *32*, 2838−2849.

DOI: 10.1021/acs.organomet.6b00422
Organometallics XXXX, XXX, XXX−XXX